Journal of Alloys and Compounds 1008 (2024) 176723

Contents lists available at ScienceDirect

Journal of Alloys and Compounds

journal homepage: www.elsevier.com/locate/jalcom

Systematic approach for high piezoelectric AlN deposition

Lucía Nieto Sierra [a,*,1], Fernando Lloret [b], Juan Jesús Gallardo [c], Carlos García Núñez [d,e], Manuel Pelayo García [d], Gonzalo Alba [a], Des Gibson [d], Daniel Araujo [a]

[a] Dpt. Materials Science, Metallurgical Engineering and Inorganic Chemistry, University of Cádiz, Puerto Real 11510, Spain
[b] Dpt. Applied Physics, University of Cádiz, Puerto Real 11510, Spain
[c] Dpt. Physical Chemistry, University of Cádiz, Puerto Real 11510, Spain
[d] Institute of Thin Films, Sensors and Imaging, University of the West of Scotland, Paisley, Scotland PA1 2BE, UK
[e] Microelectronics Lab, James Watt School of Engineering, University of Glasgow, Glasgow, Scotland G12 8QQ, UK

ARTICLE INFO

Keywords:
Vapor deposition
Crystal structure
Microstructure
Piezoelectricity
Transmission electron microscopy

ABSTRACT

Aluminum nitride (AlN) is a wide band gap semiconductor with interesting piezoelectric properties for many applications, including micromechanical systems (MEMS), acoustic wave sensors or energy harvesting devices. The influence of DC reactive magnetron sputtering (DCRMS) deposition parameters on the structural, crystalline, and piezoelectric properties of AlN thin films are presented. The systematic approach of Design of Experiments (DoE) has been used to evaluate the role of magnetron power, nitrogen and argon flows on the deposition process and the film properties. Magnetron power and argon flow have resulted to be the parameters causing the most significant effects on the deposition rate. AlN films have been deposited with a high crystal quality, showing low values of FWHM (0.28) and c-axis orientation parallel oriented respect to the growth direction, as evidenced by X-ray diffraction (XRD) analysis and high-resolution transmission electron microscopy (HRTEM). These samples also showed a high piezoelectric coefficient (d_{33}) of 5 pC/N for AlN thin films. This work highlights the importance of deposition parameters on the properties of the film and the important role that DoE play for its optimization with a minimum number of depositions.

1. Introduction

Aluminum nitride (AlN) is a wide bandgap (6.2 eV [1]) semiconductor compound with outstanding properties for many applications [2–4]. This metal nitride is an excellent candidate for the fabrication of electronic devices thanks to its high thermal conductivity of 200 W m^{-1} K^1 [5] combined with its superior insulating properties (range of $\rho = 10^9$–$10^{11}\Omega$m) [6]. Additionally, AlN can be deposited as a thin film, which makes this material a potential candidate for developing micro/nano devices and wearable/flexible electronic devices and sensors [7]. As a consequence of reducing the thickness (t <10 μm), these devices are able to operate at high frequencies [8], opening opportunities for AlN thin film devices to contribute in the area of MHz or even GHz [9,10]. Furthermore, the non-centrosymmetric character of AlN wurtzite structure (i.e., the crystal structure lacks inversion symmetry), exhibiting a strong piezoelectric coefficient along its c-axis (d_{33}) ranging from 3.4 to 5.2 pC/N for the case of polycrystalline films [11], makes it a very interesting material for a number of applications. For example, AlN function as an active layer in a variety of microelectromechanical systems (MEMS) [12] based sensors and actuators [13]. AlN has been also deposited on diamond for high-frequency surface acoustic wave (SAW) devices [14,15], taking advantage of electromechanical coupling properties, making AlN to improve the acoustic impedance between both materials. AlN has also demonstrated great potential in SAW devices for microfluidic applications, which is required in areas such as biochemical sensing or drug development [16]. Moreover, AlN has been proposed as an excellent candidate for the development of energy harvesting devices [17] with the aim of generating and storing electric power at micro-scale [18], contributing to improve the autonomy and reduce the size of the wireless sensors systems. For instance, a MEMS-based vibration energy harvester with AlN piezoelectric thin film has an output power density of 854.55 μW/(cm^3·g^2) [19].

* Corresponding author.
E-mail addresses: lucia.nieto@uca.es (L. Nieto Sierra), fernando.lloret@uca.es (F. Lloret), jj.gallardo@uca.es (J.J. Gallardo), Carlos.GarciaNunez@glasgow.ac.uk (C. García Núñez), Manuel.Pelayo@uws.ac.uk (M. Pelayo García), gonzalo.alba@uca.es (G. Alba), des.gibson@uws.ac.uk (D. Gibson), daniel.araujo@uca.es (D. Araujo).
[1] https://orcid.org/0000-0003-0052-1220

https://doi.org/10.1016/j.jallcom.2024.176723
Received 24 June 2024; Received in revised form 31 August 2024; Accepted 25 September 2024
Available online 26 September 2024

Most of the aforementioned applications strongly depend on the piezoelectric properties of AlN. In this regard, optimization of AlN film microstructure is crucial in order to achieve high quality piezoelectric properties, where d_{33} coefficient is enhanced as the (002) orientation in the wurtzite hexagonal structure of the AlN crystal is maximized [20]. However, the d_{33} coefficient has not been analyzed as a function of other AlN properties studied in this work, such as grain size and orientation, and chemical composition and stoichiometry, where pure AlN preventing oxygen incorporation inside the crystal lattice is desirable to achieve maximum d_{33}. Achieving AlN thin films with a crystal structure well-oriented along c-axis, i.e., <0001> direction in wurtzite nomenclature, is still very challenging due to the unintentional incorporation of oxygen inside the AlN structure observed in standard physical vapor deposition (PVD) procedures. That oxygen contamination as well as other microstructural factors such as grain size reduction/increase, and lattice strain [21] have been demonstrated to reduce the full width at half maximum (FWHM) of (002) peak in AlN [22]. To overcome this challenge, a thorough investigation of the AlN growth kinetics has been carried out using various techniques, including reactive direct current (DC) [23], reactive pulsed DC [24], reactive radio frequency (RF) [25] magnetron sputtering, metal-organic chemical vapour deposition (MOCVD) [26], and molecular beam epitaxy (MBE)[20,27]. Sputtering, is a PVD method capable to produce high crystal quality thin films at moderately low substrate temperatures (< 100℃ [28]) which is an advantage in comparison to its counterparts CVD (> 500℃) [26], and MBE (700℃ to 1000℃) [29]. That feature makes PVD depositions be compatible with non-conventional substrates for flexible/stretchable electronics and energy systems [30]. Among the sputtering techniques, DC reactive sputtering presents higher deposition rates (30 nm/min) [5], producing microns depositions in a relatively short time, preserving the quality. This is useful for ultrasonic applications, where 10–20 μm is needed for transducers. For optical coatings, depositing large area coatings with uniformity is key. For energy systems, it is important to have thick films that allows to add more charges into the system. These applications would not be viable achieved by epitaxial systems with very slow deposition rates. The characteristics of AlN films and the efficiency of the resulting devices can be improved by optimizing the deposition parameters. Therefore, several sputtering parameters such as gas flow/composition, residual/growth pressure, substrate temperature, and magnetron power can affect the deposition rate, modify the film characteristics an alter the crystallinity and the piezoelectric properties of the AlN film [31]. Distance between substrate and target, and purity of the target and gases, are also key parameters to control the quality of the resulting AlN thin films. From literature, the relationship between growth parameters and material properties is still not clear and might involve a huge number of samples to extract conclusions [4,5,32–35]. Regarding the gas flow for example, it can affect the full width at half maximum (FWHM) of XRD peaks of the deposited AlN films. For instance, some studies mention that by increasing the nitrogen flow ratio, the intensity of the (002) peak increases and the FWHM of the peak decreases [4]. Other works defend that a (002) preferred orientation can be achieved by deposition processes with a higher concentration of argon than nitrogen [32]. A similar ambiguity is found when the parameter under study is the magnetron power. While some studies report a better crystalline quality of AlN layers by increasing the power [33], other publications propose that a reduction in the power results in a enhancement of the (002) orientation [34]. Table 1 shows a comparison of the FWHM (XRD) of the (002) orientation of AlN films deposited under different conditions of power and Ar and nitrogen flow. The last row corresponds to the data obtained in this work for the FWHM obtained for the (002) XRD diffraction peak for sample #S1.

Table 1
Comparison of FWHM of (002) AlN obtained at different DC sputtering conditions.

	Power (W)	Ar (sccm)	N_2 (sccm)	FWHM (002)
X. Bi et al. [23]	460	3	20	1.63
A. Pandey et al. [36]	100	10	10	4.20
A. Iqbal et al. [32]	1200	40	10	2.00
This work	400	20	40	0.28

This work aims to understand the influence of sputtering parameters on the properties of AlN thin films, allowing to clarify aforementioned controversy, in order to obtain high quality and uniform AlN films for piezoelectric applications. To that end, design of experiments (DoE), being a statistical method, has been used here to analyze the effect of sputtering influential parameters on outcome material properties (or also known as DoE response variables). DoE is a mathematical statistical method that is used for optimizing a process, identifying influential factors, and studying interactions between variables. It has been applied in different scientific research such as pharmaceutical development [37], analytical chemistry and process engineering [38]. In addition, DoE techniques have also been applied to optimize the deposition parameters for various thin films including Sm-Co or ZnO:Al, among others [39].

In this work, a series of depositions have been carried out by DC reactive magnetron sputtering method using DoE to plan the deposition conditions (magnetron power, N_2 flow and Ar flow) of AlN thin films. The ultimate goal is to tune sputtering parameters in order to enhance the piezoelectric response of AlN film whilst understanding the influence of those parameters on other material properties such as crystal structure, morphology, and composition.

2. Material and methods

AlN thin films were deposited by DC reactive magnetron sputtering (Nordiko Ltd, UK) from a 100 × 300 mm^2 Al target (99.99 % purity) using N_2 and Ar as process gases. The layers were deposited on 0.80-inch single side polished (100)-oriented Si substrates (from University Wafer®). Prior to each deposition, substrates were cleaned in an ultrasonic cleaning system (UCS, from Optimal Technologies®) consisting in a series of ultrasonic baths, comprising: (i) 5 minutes in Decon neutracon® solvent (anionic and non-ionic active surface agents in an aqueous polyhydric alcohol base); (ii) 5 minutes in WashBryte® solvent: 15–30 % anionic surfactants; (iii) 5 minutes in deionized (DI) water. Finally, substrates were dried under N_2 flow and loaded into the deposition system under a residual pressure around 10^{-7} mbar, to prevent air contamination. Prior to each deposition, and with the shutter covering the substrate set in close position, the Al target was cleaned in pure Ar (flow of 30 sccm) at 300 W for 10 min to remove potential oxygen contamination from the surface, followed by 5 min carried out in a reactive atmosphere (i.e., Ar/N_2 plasma) to reach stable reactive conditions of the plasma, the latter similar to that used during the depositions. This key step allowed to achieve a stable plasma ensuring a repeatable deposition process with a constant deposition rate, and a uniform resulting thin film as it will be presented in the results section.

The deposition series have been planned via DoE through R-code software (R 4.2.1 version, from Bell Laboratories Inc.) [40], using magnetron power, N_2 gas flow, and Ar gas flow as key input variables (KIV). R software provided a wide variety of statistical and graphical techniques such as linear and nonlinear modelling, classical statistical tests or clustering among a wide variety of techniques. In this work, DoE approach involving the utilization of an upper and lower limit of each growth parameter i.e., 2-levels study was used, that corresponds therefore to a linear modelling. Specifically, AlN thin films were deposited using magnetron powers of 70 and 400 W, and Ar & N_2 flows of 20 and 40 sccm limits as summarized in Table 2.

All experiments were conducted at room temperature, and the deposition time was set at two hours. Sample S5 has not been carried out since plasma was not stable under those conditions. In order to check the repeatability of the deposition rate of the samples *see* Table S1 in Section A of Supplementary Material.

Table 2
Deposition conditions and deposition rate of samples.

Sample	Power (W)	Ar flow (sccm)	N_2 flow (sccm)	Deposition rate (nm/min)
S1	400	20	40	4.98
S2	400	40	20	8.70
S3	400	40	40	5.28
S4	70	40	20	2.34
S5	400	20	20	0.00
S6	70	20	40	1.02
S7	70	20	20	0.84
S8	70	40	40	0.84

After the deposition, samples were characterized through different techniques. The thicknesses of the deposited layers, and hence the deposition rate (Table 2), were obtained by profilometry (Dektak 3ST surface profilometer from Veeco®). Scanning electron microscopy (SEM) and energy dispersive X-ray spectroscopy (EDX) have been carried out in a VEGA 4 from Tescan to study the film morphology and the elemental composition, respectively, operating at 5 keV and 300 pA. The film crystallinity has been studied by XRD using a Siemens D5000 X-Ray diffractometer (Cu Kα, 1.5406 Å) at 40 kV/30 mA. The measures were performed in the thin films, in symmetric diffraction geometry, collecting Bragg reflections with a 2D detector. The XRD analysis has been carried out using PANalytical X'Pert HighScore Plus software. In addition, TEM studies have been carried out in a FEI Talos F200X microscope, operating at 200 keV and working in bright field (BF) and dark field (DF) mode. The elemental composition along the cross-section has been studied by Scanning-Transmission electron microscopy (STEM) EDX, using high angle annular dark field (HAADF) detector [41]. TEM analysis has been carried out through Velox software from ThermoFisher®. The cross-sectional TEM samples were prepared by lift-off method in a focused ion beam (FIB) dual beam SEM microscope from Tescan, using platinum as protective layer to prepare the lamella [42]. Finally, the piezoelectric properties have been studied by measuring the d_{33} coefficient through a Berlincourt method (PM-300 from Piezotest Ltd) adapted for thin film characterization [43]. This quasi-static method is based on the measurement of the charge generated in the piezoelectric material under the influence of an oscillating mechanical force [44].

3. Results and discussion

Fig. 1 shows the half-normal probability plot obtained from the influence of KIV (i.e., magnetron power, Ar gas flow, and N_2 gas flow) and the interaction between them, on the deposition rate (referred in DoE as key output variable, KOV) of the AlN thin films obtained from the profilometry measurements (*see* Table 2). This plot compares the absolute value of the effect from each KIV (circles in Fig. 1) and their interactions (squares in Fig. 1), on the probability scale [45] (see Section B of Supplementary Material for further discussion about the half normal plot). For a given factor, the absolute effect is the difference of the average response variable over high factor levels $\overline{X}(+)$ minus the average response over the low factor levels $\overline{X}(-)$. The absolute effect is calculated by

$$\text{Estimated effect} = \overline{X}(+) - \overline{X}(-) \quad (1)$$

Where $\overline{X}(+)$ and $\overline{X}(-)$ are high and low factor levels, respectively.

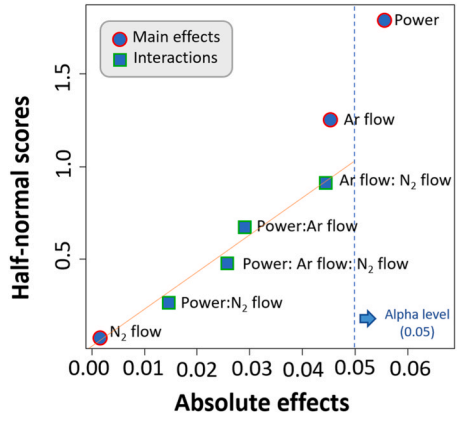

Fig. 1. DoE half-normal probability plot, for deposition rates (KOV) obtained under different deposition conditions (KIV). Each factor (magnetron power, N_2 flow and Ar flow) is represented in terms of its half normal score comprising their absolute effect (○) and interactions (□). The linear fitting evidences the significant effects; dashed line indicates the position of the alpha level.

The half normal scores represent the positions of the effects in a mean normal distribution. If the effects are not significant, they should line roughly in a straight line. Linearity implies half-normality, which implies that factors are unimportant.As a result, high-effect terms would fall near the right side of the graph an deviate from the rest of terms [46]. If the points are above the line will often indicate a positive effect, which means higher values of the corresponding KIV will contribute positive to KOVs. The orange line in Fig. 1 is a way to visualize how all the factors and factor interactions are aligned along a line (following a normal distribution) except one factor, which is the factor that have a stronger effect on the deposition rate, in this case the power (*see* Supplementary Material-Section C).

Here, the DoE demonstrates that both magnetron power and Ar flow are the KIV that most affect the growth rate of the AlN, as are the points that deviate from the line-orange line in Fig. 1. Moreover, power is the only parameter above the alpha level in the half normal scores (0.05). These results are in agreement with those observed by Y.Bian et al., that shows the high influence of power in the deposition rate [47]. In this case, as power and Ar flow points are above the line, more power or Ar flow will produce thicker layers. These results allow to calibrate the deposition rate by tuning the power level and Ar flow (Table 2). Moreover, AlN tensile stress and stoichiometry is influenced by the deposition rate [48].

Fig. 2(a-g) shows the SEM-EDX spectrum obtained at the surface of samples. For samples #S1, #S2 and #S3, the main peaks correspond to Al and N atoms. In addition, a minor contribution of oxygen (O) is also evidenced. On the other hand, samples S4-S8 have a higher intensity of the oxygen peak. Fig. 2(h) shows the N/Al ratio (left axis), obtained through the atomic percentage of nitrogen (N) divided by the atomic percentage of aluminum (Al), and the atomic percentage of oxygen (O) on the right axis. This work shows that samples with a higher percentage of nitrogen incorporated in the film are the ones deposited at higher power (i.e., higher deposition rates). In this regard, samples S1 (4.98 nm/min), S2 (8.70 nm/min) and S3 (5.28 nm/min) exhibit N/Al ratio of around 1, which corresponds to highly stoichiometric crystals (*see* green dashed line in Fig. 2(h)). Good results are obtained here for both high fluxes and low fluxes. On the other hand, samples S4 (2.34 nm/min), S6 (1.02 nm/min) and S8 (0.84 nm/min) show a higher percentage of oxygen in the film structure leading to a stoichiometry highly differing from the ideal 1:1. Sample S7 shows a N:Al stoichiometry closer to 1:1, however the presence of oxygen is quite high, around 25 %. The presence of oxygen is explained in terms of the strong chemical affinity of the Al to oxygen, that is higher than the one corresponding to nitrogen [5]. This affinity is responsible of the oxygen incorporation in samples that have less nitrogen in their structure when samples are exposed to the atmosphere [49]. Samples deposited at lower powers have more porosity as a consequence of lower energy of ions and a lower density of ions, which enhance the post-oxidation effects in porous layers.

Fig. 3 shows the XRD spectra of samples. Samples S1, S2 and S3 are the only ones among all samples exhibiting diffraction peaks corresponding to a crystalline phase of AlN. Diffractograms S4-S8 do not show

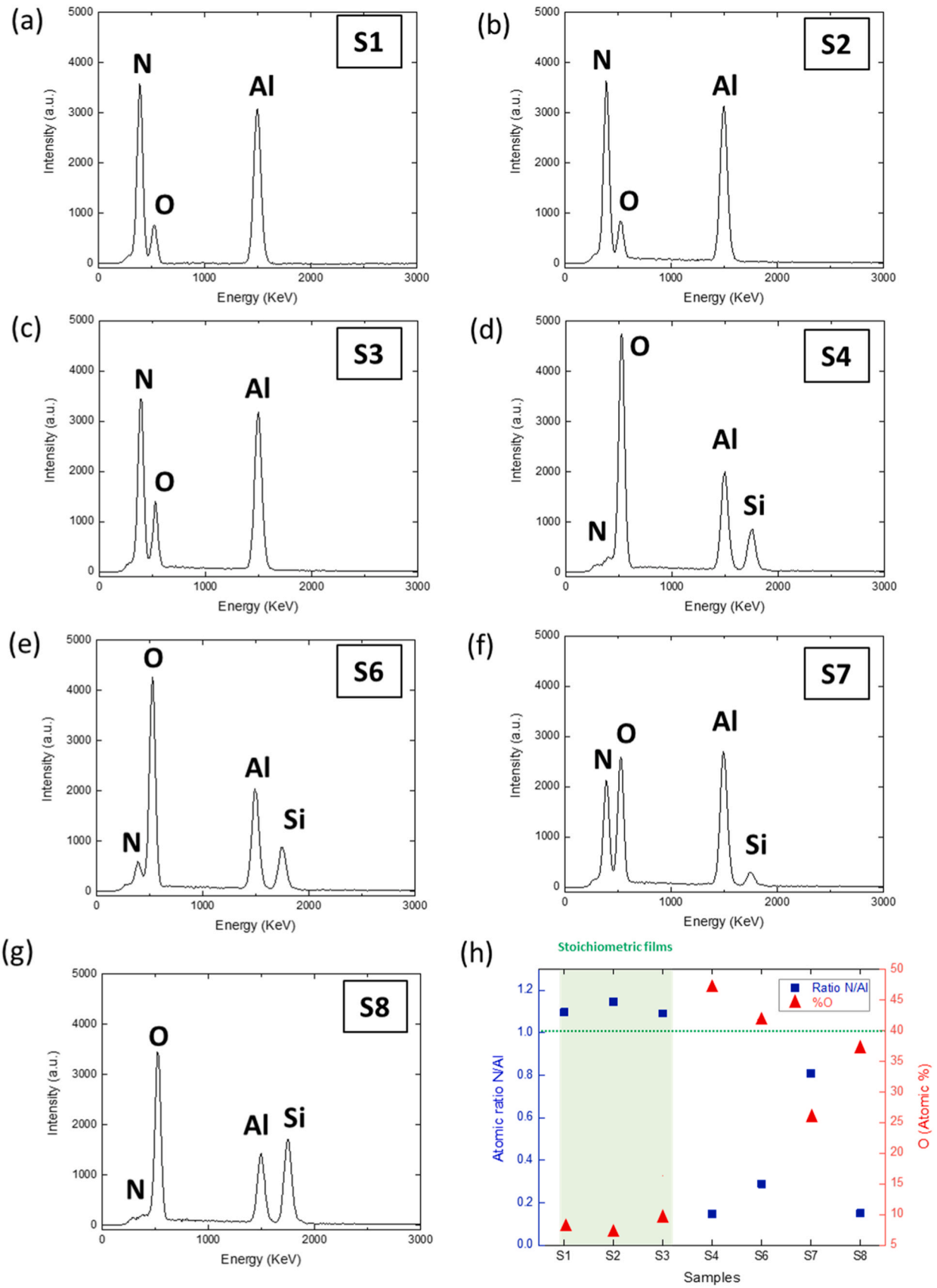

Fig. 2. (a-g) SEM-EDX spectrum of the surface of samples S1-S8, operating at 5 KeV, 300pA. (h) Graphic of SEM-EDX results extracted from samples spectra of Fig. 2 (a-g). These EDX results are shown in terms of the atomic concentration at the surface of the samples. Left axis shows the atomic ratio N/Al, and the right axis the atomic percentage of oxygen. The green area corresponds to stoichiometric films: S1, S2 and S3 are the samples with a stoichiometry closer to 1:1 N:Al, and less oxygen on the sample surface. On the other hand, samples S4-S8 present a higher oxygen incorporation.

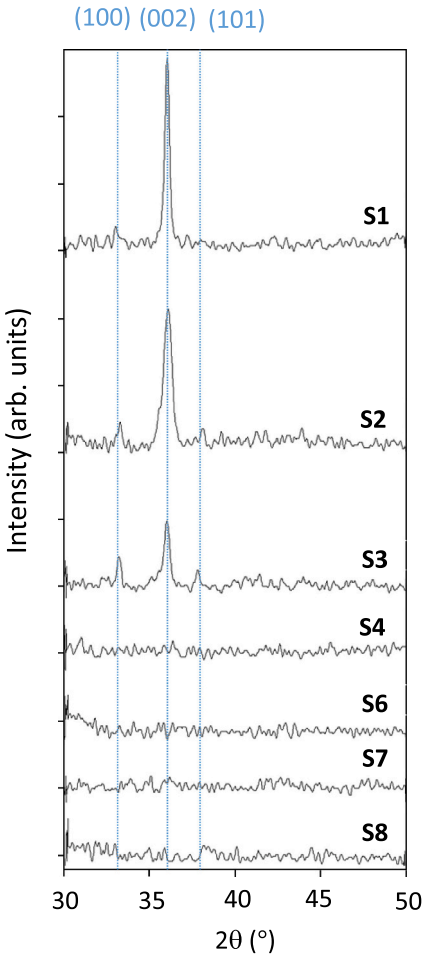

Fig. 3. XRD spectra of AlN films of samples #S1, #S2, #S3, #S4, #S6, #S7 and #S8 deposited by DC reactive sputtering at different Ar and N_2 flows.

any diffraction peak. This absence of crystallinity is attributed to the presence of an amorphous alumina (Al_xO_y), as a result of the oxygen contamination. Regarding S1, S2 and S3, the major diffraction peak is observed around $2\theta = 36.06°$ corresponds to (002) plane, characteristic of the wurtzite structure of AlN (extracted from Inorganic Crystal Structure Database (ICSD) nº 54697 [50]). Sample S1 shows (002) peak centered at that $2\theta = 36.00°$, whereas both #S2 and #S3 present (002) diffraction peak located at slightly lower angle (35.98°), indicating an increase of the tensile stress on the film [51,52]. Furthermore, (002) peak is wider in #S2 and #S3 than in #S1, which means a smaller crystallite size in #S2 and #S3 [53]. The FWHM of (002) peak shows low values on these samples, being 0.28, 0.43 and 0.32 for S1, S2 and S3 respectively. In a first order approximation, a reduction of the FWHM indicates larger grain size [54]. Although samples have different thickness, a relative comparison of the FWHM indicates that sample S1 is the one showing bigger grains as it has a higher FWHM than S2 and S3. In terms of relative intensities, S1, S2 and S3 samples present 100 % for (002) orientation. Moreover, minimal diffraction signals are detected, mainly in samples #S2 and #S3, corresponding to AlN (100), at $2\theta = 33.204°$and to AlN (101) at $2\theta = 37.734°$. Sample S2 shows a relative intensity of 17 % for (100) and 7 % for (101), while S3 shows 50 % for (100) and 31 % for (101). These relative intensities deviate from the reference values that are 100 % for (100), 65 % for (002) and 86 % for (101). These signals confirm the presence of a polycrystalline phase of the deposited film. Additionally, samples #S2 and #S3 have shoulders in the (002) peak, which can be a consequence of crystal strain or heterogeneous grain size in the layer. Consequently, XRD confirms the crystallinity of these 3 samples. To sum up, samples #S1, #S2 and #S3, which are the samples that have more nitrogen incorporated and were deposited at higher deposition speeds, show the peak corresponding to the c-axis, (002) direction. This direction is where the polarization vector is stronger and it is related to the d_{33} piezoelectric coefficient, which is the largest among all the d_{ij} [11].

Fig. 4 shows TEM micrographs in BF mode of the sputtered AlN thin films with high stoichiometry and low oxygen content, i.e., those deposited under of #S1, #S2 and #S3 conditions (*see* Table 2). Specifically, (a-c) present HRTEM micrographs of the AlN films and Fig. 4(d-f) their corresponding fast-Fourier transform (FFT). Fig. 4(a-c) show Moiré fringes, resulting from the interference of two sets of planes. This result corroborates the presence of different orientations in the film [55]. By measuring in the FFT pattern the distance between the main spots and its symmetrical, the interplanar distance is calculated. From these measurements, the deduced interplanar distances are 0.27, 0.25 and 0.24 nm which corresponds to the (100), (002) and (101) families, respectively. Moreover, it is possible to do an approach of the grain size by comparing the FFT patterns. Fig. 4(d) shows a ring pattern with more defined spots than Fig. 4(e) and (f), where the patterns are well defined Debye-Scherrer rings [56]. This indicates that #S1 presents wider grains than #S2 and #S3. This result is in agreement with those obtained in XRD, where S1 was the sample with lower FWHM, which indicates a bigger grain size.

Fig. 4 h shows the FFT of the grains of Fig. 4 g. In this area, a pattern corresponding to the [010] pole is identified (Fig. 4i). Indeed, the N/L and M/L ratios corresponds to the ratios obtained from the theoretical pattern. Therefore, the TEM lamella is parallel to the (010) planes of a family of grains. These grains have their c-axis (direction [001]) perpendicular to the AlN/Si interface. Specifically, the presence of (002) orientation is crucial, as this orientation is the main responsible of the piezoelectric properties of the film [57].

Fig. 5 shows Selected Area Electron Diffraction (SAED), DF-TEM micrographs of samples (a) #S1, (#b) #S2 and (c) #S3 recorded using the [002], [100] and [101] reflections. SAED technique selects just a certain area of the sample by inserting an aperture (10 μm) above the specimen [55,58]. Additionally, the use of an objective aperture allows to select a specific spot of the diffraction pattern, i.e., a specific reflection. Therefore, the contribution of only such reflection of the AlN layer shows up. This allows to select a AlN related reflection [59]. The corresponding diffraction patterns obtained from the AlN layer are shown as inset. These diffraction patterns show a ring pattern where each ring corresponds to a certain family of plains. This corroborates the presence of polycrystalline AlN. The main observed rings correspond to the family of plains (002), (100) and (101). The blue circumference marks the position of the objective aperture used for the DF micrograph. In these cases, the objective aperture is centered in the (002) spot. However, the smallest objective aperture available (10 μm) is too big to select just the contribution of a single spot from the diffraction pattern, so the selected point covers the contributions of spots belonging to three different rings: (002), (100) and (101).

Regarding the grain orientation in Fig. 5, the upper part of the layer exhibits larger columnar grains perpendicular to the Si substrate. Most of the grains that are illuminated have (002) orientation as the aperture is centered in that spot [60]. Therefore, these layers have columnar grains with its c-axis perpendicular to the Si surface, which is adequate for the piezoelectric response. Additionally, sample #S3 shows slightly tilted grains, 15º respect the c-axis, measured by ImageJ software [61]. This is explained in terms of the different deposition conditions compared to samples #S1 and #S2. #S3 has been deposited at a higher pressure ($4.15{\cdot}10^{-3}$ mbar) than #S1 and #S2 ($3.4{\cdot}10^{-3}$ and $3.33{\cdot}10^{-3}$ mbar, respectively), as its total gas flow is 80 sccm, compared to the 60 sccm of total gas flow of #S1 and #S2. A higher pressure is traduced in a smaller free path of the atoms, so the sputtering particles will make collisions before reaching the substrate and the probability of forming dimmers is higher, reducing therefore the energy of the particles. These phenomena will enhance the growth of (100) direction, instead of the

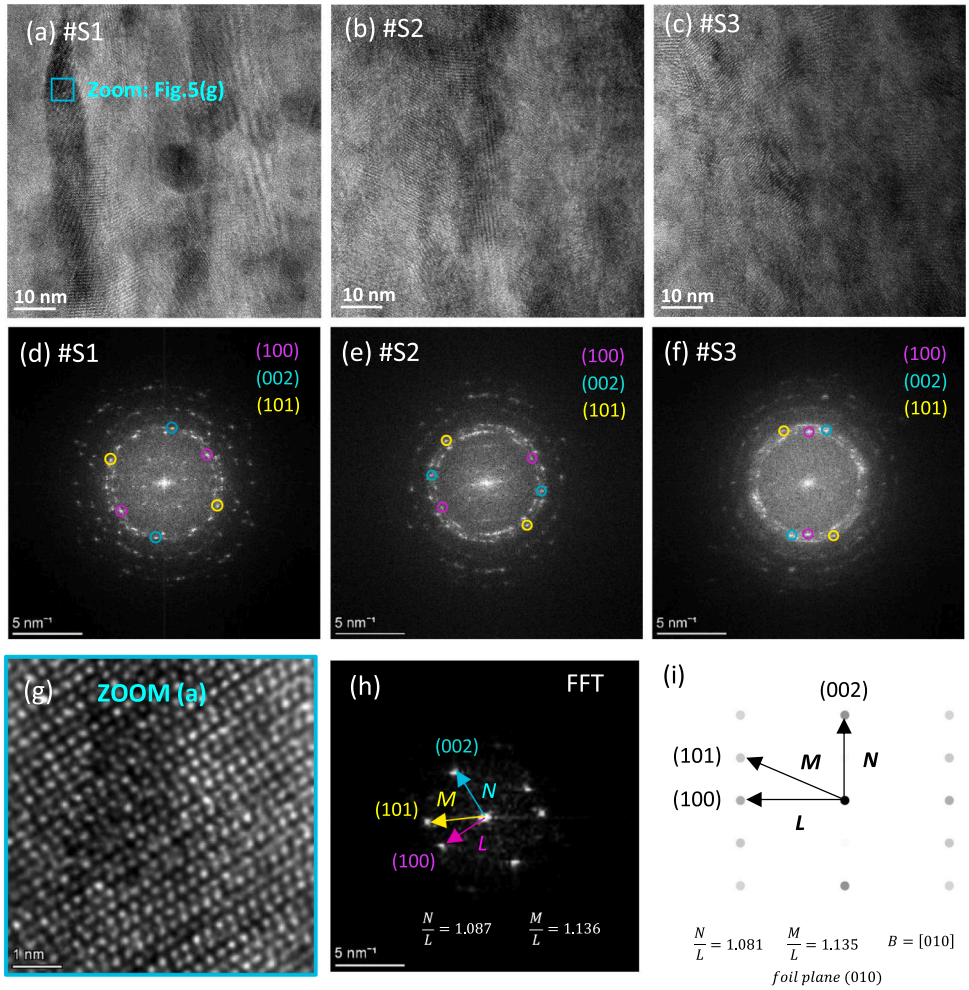

Fig. 4. (a), (b), (c) HRTEM micrographs of samples #S1, #S2 and #S3, respectively, using BF mode and (d), (e), (f) their corresponding FFT, operating at 200 KeV. Main orientations are marked by coloured circumferences, pink for (100) orientation, blue for (002) and yellow for (101). (g) Zoom of a grain of Fig. 4(a). (h) FFT of Fig. 4(h), (i) Standard indexed diffraction patterns for hcp crystal in $B = [010]$ beam direction. Ratios of the principal spots spacing are shown.

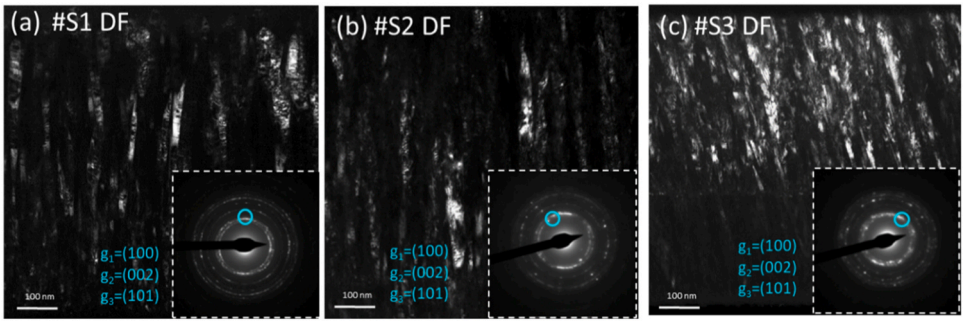

Fig. 5. Cross sectional Dark Field TEM micrographs of the AlN layer of samples (a) #S1, (b) #S2 and (c) #S3. The diffraction patterns of the layer are shown as insets with the selected spot marked by blue circumferences. These circumferences collect (100), (002) and (101) orientations.

c-axis direction (002), as the Al-N bond in the direction of the c-axis is higher [62]. Thus, tilted AlN film is deposited [63]. These results agree with XRD results, as the diffractogram #S3 shows a diffraction peak at 2θ= 33.204, that corresponds to (100) orientation.

Fig. 6(a) is a HRTEM micrograph of sample #S1 in cross-sectional view, showing the AlN/Si interface. Three sections are distinguished in this micrograph: AlN polycrystalline phase on the top (Zoom 1), an amorphous phase as interlayer (Zoom 2), and Si (100) substrate (Zoom 3). Each zoom has its corresponding FFT, comprising Zoom1-FFT1, Zoom2-FFT2, and Zoom 3-FFT3 presented in Fig. 6(e,d,f), respectively. FFT2-which is the FFT of the Zoom 2- shows less spots than FFT1 and contributions of an amorphous phase, as it shows amorphous circles, different from the polycrystalline rings observed in FFT1. These polycrystalline rings correspond to the same rings observed in Fig. 4(d) for AlN orientation. On the other hand, regarding the grain size, Cutout 1, and Cutout 2 of Fig. 6 show areas, pointed out with a dashed circumference, where grains of the indicated size are revealed. The deposited film has been divided in two sections for this purpose (Cutout 1 in Fig. 6(b), and Cutout 2 in Fig. 6(c)) as there is a clear difference between the grain size of the very first nanometers (∼ 10nm) of the

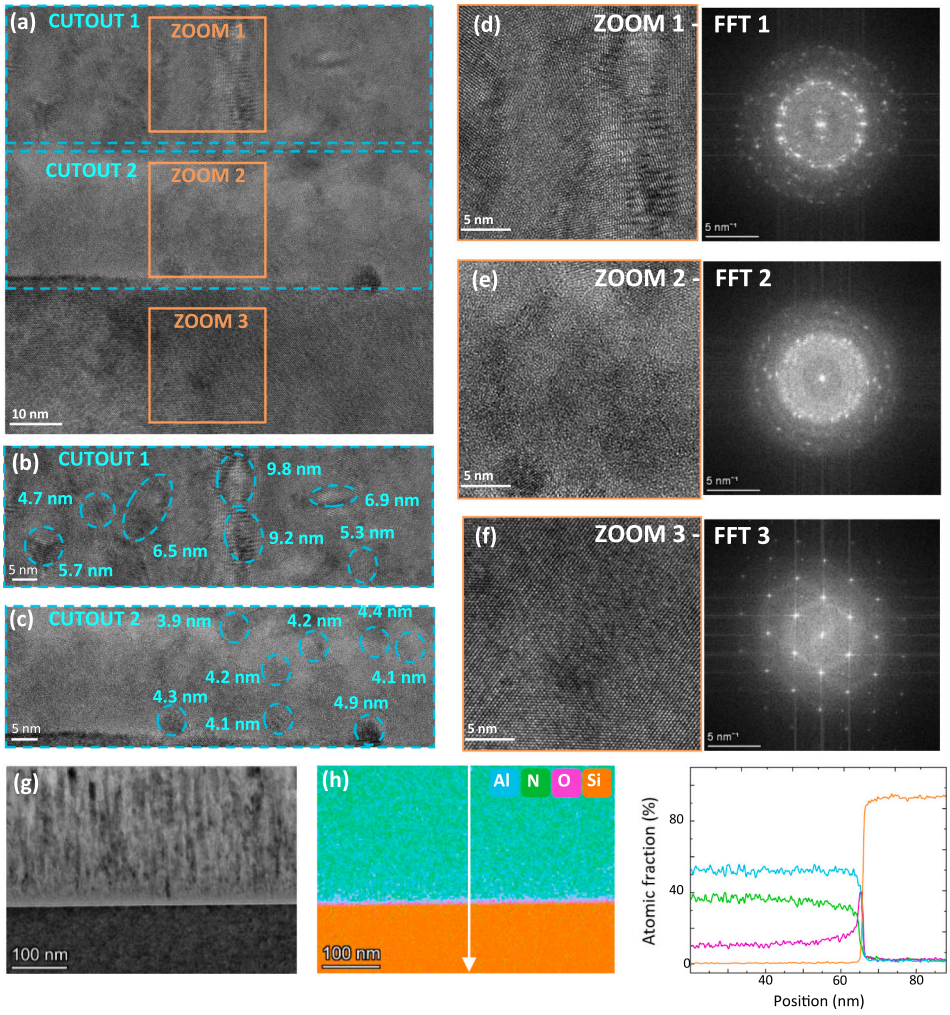

Fig. 6. (a) Cross sectional HRTEM micrograph of the interface of sample #S1. (b) Cutout 1: AlN layer showing examples grains of 5–10 nm (pointed out with dashed blue circumferences). (c) Cutout 2: AlN/Si interlayer showing examples of grains of <5 nm (pointed out with dashed blue circumferences). (d) Zoom 1-FFT1: AlN polycrystalline phase, (e) Zoom 2-FFT2: a mixture of small grains of AlN and an amorphous phase, (f) Zoom 3-FFT3: Si (100) substrate, (g) STEM micrograph obtained by the application of EDX technique in #S1, (h) Coloured map of S1 obtained from the STEM micrograph of Fig. 6(g) and the corresponding profile intensity in the direction of the white arrow.

deposited film and the grain size of the rest of it [64]. The section of Cutout 1 shows larger grains (> 5 nm) than the grains observed in Cutout 2 (<5 nm). These results agree with those of FFT, as FFT1 shows more distinguished spots than FFT2, which indicates a larger grain size.

Additionally, EDX through STEM has been carried out to study the elemental composition along the layer of sample #S1 (Fig. 6(g) STEM micrograph using HAADF detector). The section corresponding to Zoom2 in Fig. 6(e) shows a composition of a higher concentration of

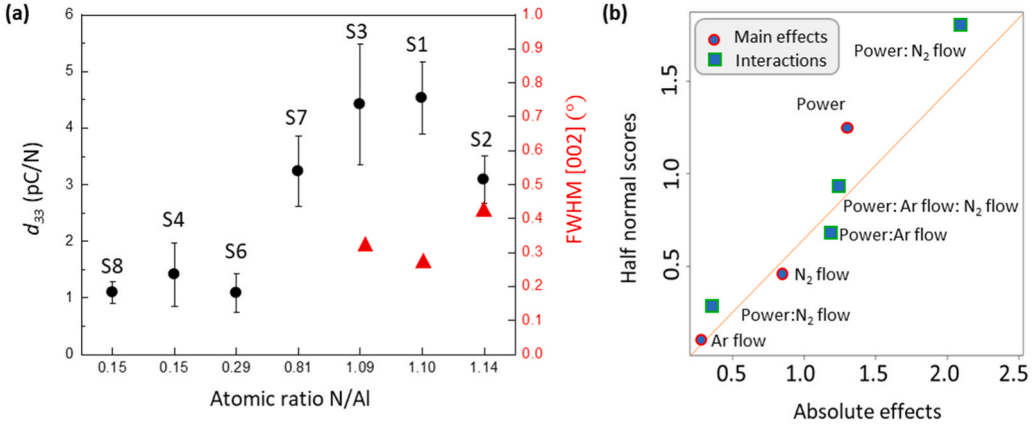

Fig. 7. (a) Left axis (black) shows d_{33} coefficient vs N/Al ratio obtained through SEM-EDX, selecting the atomic % of each element, right axis (red) shows the FWHM for (002) of samples S1, S2 and S3. (b) DoE half normal probability plot for d_{33} coefficient obtained under different DC sputtering deposition conditions.

oxygen than nitrogen, being the opposite composition of Zoom1 (Fig. 6 (d)), that presents a higher concentration of nitrogen than oxygen. This HRTEM micrograph indicates that the interlayer of sample #S1 observed in Fig. 6(c) (Cutout 2) corresponds to small grains of AlN (<5 nm) in a matrix of an amorphous phase of $Al_xN_yO_z$. The presence of oxygen on this part of the layer is probably due to the native oxide of silicon has not been eliminated on the cleaning process, and as a consequence, this oxygen react with the Al-N particles that arrive on Si substrate at the initial stage of film deposition [65]. The native oxygen on Si (100) along with the residual oxygen in the reaction chamber and the low deposition temperature have produced this interlayer, as is reported by Hwang et al. [66].

Fig. 7(a) presents d_{33} coefficient measured in AlN thin films with different stoichiometries, i.e., N/Al ratios (*see* EDX analysis above). From that study, one could easily understand that samples with a better stoichiometry, i.e., samples with a N/Al ratio closer to 1 (S1, S2 and S3), are those AlN thin films exhibiting a higher d_{33} coefficient of around 4.5–5 pC/N. Not only the N/Al ratio is important for the piezoelectric effect, but also the oxygen concentration. The piezoelectric properties of films deposited through a sputtering process are significantly impacted by the concentration of oxygen, as there is a greater propensity for Al atoms to form bonds with O atoms and consequently, modify the crystallinity [11]. These results are in good agreement with those of the XRD and TEM, as the samples that present a higher d_{33} coefficient match with the ones that show good (002) orientation. This fact is explained in terms of the strong relation between piezoelectricity and crystallinity. A c-axis (002) orientation of the hexagonal AlN is necessary for enhance the d_{33} coefficient of the material [67,68]. Furthermore, as reported by Fei et al., the piezoelectric stress constant is significantly influenced by the c-axis and the (002) orientation distribution [11]. Additionally, the slightly titling angle observed in sample S3 (Fig. 5(c)) may have reduced the d_{33} coefficient, i.e., the effective d_{33} is reduced by a factor $\cos\gamma$, where γ is the angle of the c-axis with respect to the substrate normal (*see* Fig. 5(c)) [69]. The mixture of grains and their size observed in HRTEM micrographs might contribute to reduce the d_{33} due to the inversion of domains as it creates dipoles in opposite directions [11].

On the other hand, in Fig. 7(b) the half normal probability plot is proposed with the aim of determining which parameter or combination of parameters has a stronger influence on the piezoelectric effect of sputtered AlN thin films. The DoE demonstrates that magnetron power combined with the nitrogen flow is the factor interaction that affects the most the d_{33} of the film, as is the factor interaction with a higher absolute effect and deviates more above the line within the power. However, these points do not affect significantly to the d_{33} as they do not deviate drastically from the line.

4. Conclusions

This work highlights the benefits of using DoE for the optimization of DC reactive magnetron sputtering deposition conditions to obtain piezoelectric AlN thin films. It explores the impact of the deposition parameters including magnetron power, nitrogen flow and argon flow on the elemental composition, the structural, crystalline, and piezoelectric properties of AlN thin films. DoE analysis revealed that the deposition rate is primarily influenced by magnetron power and Ar flow. The deposition rate has been taken into account as KOV as it influences the film properties in terms of impurity incorporation and tensile stress [5].

This work demonstrates that AlN thin films with high-crystal quality and c-axis (002) well-oriented with growth direction is achieved by using a power of 400 W, 20 sccm of Ar flow and 40 sccm of N_2 flow. It is stablished that increase of N_2 flow produce films with better crystallinity (lower FWHM) and increase of Ar flow also enhance the (100) orientation.

SEM-EDX analysis indicated that higher nitrogen incorporation is obtained at a higher power (400 W). XRD and TEM analysis have confirmed the crystalline nature of samples #S1 (400 W, 20:40 Ar:N_2), #S2 (400 W, 40:20 Ar:N_2) and #S3 (400 W, 40:40 Ar:N_2), which show a well oriented c-axis orientation (002), i.e. aligned with the crystal growth direction. However, sample S3 conditions produce tilting, which slightly reduce the effective d_{33} as gamma angle is off-tilt. Moreover, the analysis of the interface shows that the first 15 nm of the layers have amorphous regions and smaller grains (<5 nm), in contrast with the rest of the film, which shows bigger and columnar grains. The d_{33} coefficient measurements have revealed that samples with better stoichiometry, lower oxygen incorporation and well oriented c-axis exhibit higher piezoelectric coefficients (4.5–5 pC/N), that confirms the connection between crystallinity and piezoelectricity. These results emphasize the importance of using the DoE approach to optimize the deposition conditions in order to obtain piezoelectric films, which is promising for the development of energy harvesting devices.

CRediT authorship contribution statement

Fernando Lloret: Writing – review & editing, Writing – original draft, Validation, Supervision, Resources, Project administration, Funding acquisition, Formal analysis, Conceptualization, Investigation. **Lucía Nieto Sierra:** Writing – review & editing, Writing – original draft, Methodology, Investigation, Formal analysis, Data curation, Software, Validation. **Des Gibson:** Project administration, Funding acquisition, Resources, Supervision. **Gonzalo Alba:** Methodology, Investigation. **Daniel Araujo:** Writing – review & editing, Resources, Project administration, Funding acquisition, Conceptualization, Supervision. **Juan Jesús Gallardo:** Writing – review & editing, Writing – original draft, Validation, Supervision, Resources, Formal analysis, Conceptualization, Funding acquisition. **Manuel Pelayo García:** Writing – review & editing, Methodology, Investigation. **Carlos García Núñez:** Writing – review & editing, Writing – original draft, Validation, Supervision, Resources, Formal analysis, Conceptualization, Methodology, Software.

Declaration of Competing Interest

The authors declare that they have no known competing financial interests or personal relationships that could have appeared to influence the work reported in this paper.

Data availability

Data will be made available on request.

Acknowledgments

This work was supported by MICINN project Aircarft wing energy harvesting through diamond based piezo systems (DiamondWings) [PID2019–110219RB-100]; MICINN project OptoFET [PID2020–117201RB-C21]; Junta Andalucía PAIDI project Volar con Diamante [PY20_00946]; MICINN project [PDC2023–145907-I00]; and Junta de Andalucía 2017 project, Carbo-Diamond [FEDER-UCA18–107851]. We would like to thank as well to the Institute of Thin Films, Sensors and Imaging at the University of the West of Scotland (UWS).

Appendix A. Supporting information

Supplementary data associated with this article can be found in the online version at doi:10.1016/j.jallcom.2024.176723.

References

[1] N. Sharma, S. Ilango, Anisotropic piezoelectric response of ion beam sputtered aluminum nitride thin films textured along [10$\bar{1}$0]-axis: A field dependent X-ray diffraction investigation, Appl. Surf. Sci. 452 (2018) 299–305, https://doi.org/10.1016/j.apsusc.2018.04.238.

[2] A. Iqbal, F. Mohd-Yasin, Reactive sputtering of aluminum nitride (002) thin films for piezoelectric applications: a review, Sensors 18 (2018) 1797, https://doi.org/10.3390/S18061797.

[3] R.M.R. Pinto, V. Gund, C. Calaza, K.K. Nagaraja, K.B. Vinayakumar, Piezoelectric aluminum nitride thin-films: A review of wet and dry etching techniques, Microelectron. Eng. 257 (2022) 111753, https://doi.org/10.1016/j.mee.2022.111753.

[4] G.F. Iriarte, J. Bjurström, J. Westlinder, F. Engelmark, I.V. Katardjiev, Synthesis of C-axis-oriented AlN thin films on high-conducting layers: Al, Mo, Ti, TiN, and Ni, IEEE Trans. Ultrason. Ferroelectr. Freq. Control 52 (2005) 1170–1174, https://doi.org/10.1109/TUFFC.2005.1504003.

[5] G.F. Iriarte, J.G. Rodríguez, F. Calle, Synthesis of c-axis oriented AlN thin films on different substrates: A review, Mater. Res. Bull. 45 (2010) 1039–1045, https://doi.org/10.1016/j.materresbull.2010.05.035.

[6] A. Pandey, J. Kaushik, S. Dutta, A.K. Kapoor, D. Kaur, Electrical and structural characteristics of sputtered c-oriented AlN thin films on Si (100) and Si (110) substrates, Thin Solid Films 666 (2018) 143–149, https://doi.org/10.1016/j.tsf.2018.09.016.

[7] G. Piazza, V. Felmetsger, P. Muralt, R.H. Olsson, R. Ruby, Piezoelectric aluminum nitride thin fi lms for microelectromechanical systems, MRS Bull. 37 (2012) 1051–1061, https://doi.org/10.1557/mrs.2012.268.

[8] H. Fiedler, V. Jovic, D.R.G. Mitchell, J. Leveneur, E. Anquillare, K.E. Smith, J. Kennedy, Tuning the electromechanical properties and polarization of Aluminium Nitride by ion beam-induced point defects, Acta Mater. 203 (2021), https://doi.org/10.1016/j.actamat.2020.116495.

[9] M. Hara, J. Kuypers, T. Abe, M. Esashi, Surface micromachined AlN thin film 2 GHz resonator for CMOS integration, Sens. Actuators, A Phys. 117 (2005) 211–216, https://doi.org/10.1016/j.sna.2004.06.014.

[10] C. Chen, Z. Shang, J. Gong, F. Zhang, H. Zhou, B. Tang, Y. Xu, C. Zhang, Y. Yang, X. Mu, Electric Field Stiffening Effect in c-Oriented Aluminum Nitride Piezoelectric Thin Films, ACS Appl. Mater. Interfaces 10 (2018) 1819–1827, https://doi.org/10.1021/acsami.7b14759.

[11] C. Fei, X. Liu, B. Zhu, D. Li, X. Yang, Y. Yang, Q. Zhou, AlN piezoelectric thin films for energy harvesting and acoustic devices, Nano Energy 51 (2018) 146–161, https://doi.org/10.1016/j.nanoen.2018.06.062.

[12] M. Noor-A-Alam, O. Z. Olszewski, M. Nolan, Ferroelectricity and Large Piezoelectric Response of AlN/ScN Superlattice, ACS Appl. Mater. Interfaces 11 (2019) 20482–20490, https://doi.org/10.1021/acsami.8b22602.

[13] X.Y. Zhang, D.C. Peng, J. Han, F.Bin Ren, S.C. Jiang, M.C. Tseng, Y.J. Ruan, J. Zuo, W.Y. Wu, D.S. Wuu, C.J. Huang, S.Y. Lien, W.Z. Zhu, Effect of substrate temperature on properties of AlN buffer layer grown by remote plasma ALD, Surf. Interfaces 36 (2023), https://doi.org/10.1016/j.surfin.2022.102589.

[14] F. Lloret, D. Araújo, M.P. Villar, J.G. Rodríguez-Madrid, G.F. Iriarte, O.A. Williams, F. Calle, Diamond underlayer microstructure effect on the orientation of AlN piezoelectric layers for high frequency SAW resonators by TEM, Microelectron. Eng. 112 (2013) 193–197, https://doi.org/10.1016/J.MEE.2013.04.007.

[15] M. Gillinger, K. Shaposhnikov, T. Knobloch, M. Stöger-Pollach, W. Artner, K. Hradil, M. Schneider, M. Kaltenbacher, U. Schmid, Enhanced c-axis orientation of aluminum nitride thin films by plasma-based pre-conditioning of sapphire substrates for SAW applications, Appl. Surf. Sci. 435 (2018) 432–437, https://doi.org/10.1016/j.apsusc.2017.11.113.

[16] J. Zhou, M. Demiguel-Ramos, L. Garcia-Gancedo, E. Iborra, J. Olivares, H. Jin, J. K. Luo, A.S. Elhady, S.R. Dong, D.M. Wang, Y.Q. Fu, Characterisation of aluminium nitride films and surface acoustic wave devices for microfluidic applications, Sens. Actuators, B Chem. 202 (2014) 984–992, https://doi.org/10.1016/j.snb.2014.05.066.

[17] T.T. Yen, T. Hirasawa, P.K. Wright, A.P. Pisano, L. Lin, Corrugated aluminum nitride energy harvesters for high energy conversion effectiveness, J. Micromech. Microeng. 21 (2011) 085037, https://doi.org/10.1088/0960-1317/21/8/085037.

[18] R. Elfrink, T.M. Kamel, M. Goedbloed, S. Matova, D. Hohlfeld, Y. Van Andel, R. Van Schaijk, Vibration energy harvesting with aluminum nitride-based piezoelectric devices, J. Micromech. Microeng. 19 (2009) 094005, https://doi.org/10.1088/0960-1317/19/9/094005.

[19] X. He, Q. Wen, Z. Lu, Z. Shang, Z. Wen, A micro-electromechanical systems based vibration energy harvester with aluminum nitride piezoelectric thin film deposited by pulsed direct-current magnetron sputtering, Appl. Energy 228 (2018) 881–890, https://doi.org/10.1016/j.apenergy.2018.07.001.

[20] H. Cheng, Y. Sun, P. Hing, Microstructure evolution of AlN films deposited under various pressures by RF reactive sputtering, Surf. Coat. Technol. 166 (2003) 231–236, https://doi.org/10.1016/S0257-8972(02)00771-5.

[21] N. Afzal, M. Devarajan, K. Ibrahim, Growth of polycrystalline indium aluminum nitride thin films on silicon (111) substrates, Mater. Sci. Semicond. Process. 27 (2014) 975–984, https://doi.org/10.1016/j.mssp.2014.08.036.

[22] F. Jose, R. Ramaseshan, S. Dash, S. Bera, A.K. Tyagi, B. Raj, Response of magnetron sputtered AlN films to controlled atmosphere annealing, J. Phys. D. Appl. Phys. 43 (2010) 075304, https://doi.org/10.1088/0022-3727/43/7/075304.

[23] X. Bi, Y. Wu, J. Wu, H. Li, L. Zhou, A model for longitudinal piezoelectric coefficient measurement of the aluminum nitride thin films, J. Mater. Sci. Mater. Electron. 25 (2014) 2435–2442, https://doi.org/10.1007/S10854-014-1885-3/FIGURES/7.

[24] M. Ohtsuka, H. Takeuchi, H. Fukuyama, Effect of sputtering pressure on crystalline quality and residual stress of AlN films deposited at 823K on nitrided sapphire substrates by pulsed DC reactive sputtering, Jpn. J. Appl. Phys. 55 (2016) 05FD08, https://doi.org/10.7567/JJAP.55.05FD08/XML.

[25] A. Taurino, M.A. Signore, M. Catalano, M.J. Kim, 1 0 1) and (0 0 2) oriented AlN thin films deposited by sputtering, Mater. Lett. 200 (2017) 18–20, https://doi.org/10.1016/J.MATLET.2017.04.081.

[26] M.A.A.Z.M. Sahar, Z. Hassan, S.S. Ng, N.A. Hamzah, Y. Yusuf, N.N. Novikova, V. A. Yakovlev, S.A. Klimin, An insight into growth transition in AlN epitaxial films produced by metal-organic chemical vapour deposition at different growth temperatures, Superlattices Micro 161 (2022) 107095, https://doi.org/10.1016/j.spmi.2021.107095.

[27] Y.H. Kim, J.H. Lee, Y.K. Noh, J.E. Oh, S.J. Ahn, Microstructural characteristics of AlN thin layers grown on Si(110) substrates by molecular beam epitaxy: Transmission electron microscopy study, Thin Solid Films 576 (2015) 61–67, https://doi.org/10.1016/j.tsf.2015.01.008.

[28] C. Perez, A.J. McLeod, M.E. Chen, S.I. Yi, S. Vaziri, R. Hood, S.T. Ueda, X. Bao, M. Asheghi, W. Park, A.A. Talin, S. Kumar, E. Pop, A.C. Kummel, K.E. Goodson, High Thermal Conductivity of Submicrometer Aluminum Nitride Thin Films Sputter-Deposited at Low Temperature, ACS Nano 17 (2023) 21240–21250, https://doi.org/10.1021/acsnano.3c05485.

[29] F. Malengreau, M. Vermeersch, S. Hagège, R. Sporken, M.D. Lange, R. Caudano, Epitaxial growth of aluminum nitride layers on Si(111) at high temperature and for different thicknesses, J. Mater. Res. 12 (1997) 175–188, https://doi.org/10.1557/JMR.1997.0024.

[30] G. Ross, H. Dong, C.B. Karuthedath, A.T. Sebastian, T. Pensala, M. Paulasto-Kröckel, The impact of residual stress on resonating piezoelectric devices, Mater. Des. 196 (2020), https://doi.org/10.1016/j.matdes.2020.109126.

[31] J.G. Rodríguez-Madrid, G.F. Iriarte, D. Araujo, M.P. Villar, O.A. Williams, W. Müller-Sebert, F. Calle, Optimization of AlN thin layers on diamond substrates for high frequency SAW resonators, Mater. Lett. 66 (2012) 339–342, https://doi.org/10.1016/J.MATLET.2011.09.003.

[32] A. Iqbal, G. Walker, L. Hold, A. Fernandes, A. Iacopi, F. Mohd-Yasin, DC sputtering of highly c-axis AlN films on top of 3C-SiC (111)-on-Si (111) substrates under various N2 concentrations, J. Vac. Sci. Technol. B, Nanotechnol. Microelectron. Mater. Process. Meas. Phenom. 35 (2017) 06GH01, https://doi.org/10.1116/1.4991748.

[33] J.X. Zhang, H. Cheng, Y.Z. Chen, A. Uddin, S. Yuan, S.J. Geng, S. Zhang, Growth of AlN films on Si (100) and Si (111) substrates by reactive magnetron sputtering, Surf. Coat. Technol. 198 (2005) 68–73, https://doi.org/10.1016/J.SURFCOAT.2004.10.075.

[34] H. Cheng, Y. Sun, P. Hing, The influence of deposition conditions on structure and morphology of aluminum nitride films deposited by radio frequency reactive sputtering, Thin Solid Films 434 (2003) 112–120, https://doi.org/10.1016/S0040-6090(03)00428-0.

[35] B. Abdallah, S. Al-Khawaja, A. Alkhawwam, I.M. Ismail, Deposition and current conduction of mixed hexagonal and cubic phases of AlN/p-Si films prepared by vacuum arc discharge: Effect of deposition temperature, Thin Solid Films 562 (2014) 152–158, https://doi.org/10.1016/j.tsf.2014.04.009.

[36] A. Pandey, S. Dutta, R. Prakash, R. Raman, A.K. Kapoor, D. Kaur, Growth and Comparison of Residual Stress of AlN Films on Silicon (100), (110) and (111) Substrates, J. Electron. Mater. 47 (2018) 1405–1413, https://doi.org/10.1007/s11664-017-5924-8.

[37] S. N. Politis, P. Colombo, G. Colombo, D. M. Rekkas, Design of experiments (DoE) in pharmaceutical development, Drug Dev. Ind. Pharm. 43 (2017) 889–901, https://doi.org/10.1080/03639045.2017.1291672.

[38] M. Akiyama, T. Tabaru, K. Nishikubo, A. Teshigahara, K. Kano, Preparation of scandium aluminum nitride thin films by using scandium aluminum alloy sputtering targetb and design of experiments, J. Ceram. Soc. Jpn. 118 (2010) 1166–1169, https://doi.org/10.2109/jcersj2.118.1166.

[39] G. Venkata Ramana, P. Saravanan, S.V. Kamat, Y. Aparna, Optimization of sputtering parameters for SmCo thin films using design of experiments, Appl. Surf. Sci. 261 (2012) 110–117, https://doi.org/10.1016/j.apsusc.2012.07.109.

[40] R Core Team R, A Language and Environment for Statistical Computing, R Foundation for Statistical Computing, Vienna, Austria, 2022. ⟨https://www.r-project.org/⟩.

[41] Y. Li, W. Liu, V. Ortalan, W.F. Li, Z. Zhang, R. Vogt, N.D. Browning, E.J. Lavernia, J.M. Schoenung, HRTEM and EELS study of aluminum nitride in nanostructured Al 5083/B4C processed via cryomilling, Acta Mater. 58 (2010) 1732–1740, https://doi.org/10.1016/j.actamat.2009.11.015.

[42] M. Sugiyama, G. Sigesato, A review of focused ion beam technology and its applications in transmission electron microscopy, J. Electron Microsc. (Tokyo). 53 (2004) 527–536, https://doi.org/10.1093/jmicro/dfh071.

[43] M.P. Garcia, D. Gibson, D.A. Hughes, C.G. Nuñez, A Refined Quasi-Static Method for Precise Determination of Piezoelectric Coefficient of Nanostructured Standard and Inclined Thin Films, 2300091 (2023) 1–12. https://doi.org/10.1002/apxr.202300091.

[44] B. Toroń, P. Szperlich, M. Nowak, A. Starczewska, A novel method for measuring piezoelectric coefficients, Measurement 206 (2023) 112274, https://doi.org/10.1016/J.MEASUREMENT.2022.112274.

[45] K. Krishnaiah, P. Shahabudeen, Applied Design of Experiments and Taguchi Methods, Eastern Ec, 2012.

[46] W. Yu, K. Sepehrnoori, An Assisted History-Matching Workflow Using a Proxy-Based Approach for Shale Reservoirs, in: Shale Gas Tight Oil Reserv. Simul., 2018: pp. 277–332. https://doi.org/10.1016/b978-0-12-813868-7.00007-9.

[47] Y. Bian, M. Liu, G. Ke, Y. Chen, J. DiBattista, E. Chan, Y. Yang, Aluminum nitride thin film growth and applications for heat dissipation, Surf. Coat. Technol. 267 (2015) 65–69, https://doi.org/10.1016/j.surfcoat.2014.11.060.

[48] G.F. Iriarte, J.G. Rodríguez, F. Calle, Synthesis of c-axis oriented AlN thin films on different substrates: A review, Mater. Res. Bull. 45 (2010) 1039–1045, https://doi.org/10.1016/J.MATERRESBULL.2010.05.035.
[49] M. Legallais, H. Mehdi, S. David, F. Bassani, S. Labau, B. Pelissier, T. Baron, E. Martinez, G. Ghibaudo, B. Salem, Improvement of AlN Film Quality Using Plasma Enhanced Atomic Layer Deposition with Substrate Biasing, ACS Appl. Mater. Interfaces 12 (2020) 39870–39880, https://doi.org/10.1021/acsami.0c10515.
[50] W. Paszkowicz, S. Podsiadło, R. Minikayev, Rietveld-refinement study of aluminium and gallium nitrides, J. Alloy. Compd. 382 (2004) 100–106, https://doi.org/10.1016/j.jallcom.2004.05.036.
[51] M. Gillinger, M. Schneider, A. Bittner, P. Nicolay, U. Schmid, Impact of annealing temperature on the mechanical and electrical properties of sputtered aluminum nitride thin films, J. Appl. Phys. 117 (2015), https://doi.org/10.1063/1.4907208.
[52] M.G. Ambartsumov, V.A. Tarala, M.S. Nikova, S.O. Krandievsky, L.V. Kozhitov, Influence of coating thickness on the microstructure, composition and optical properties of aluminum nitride thin films grown on silicon substrates via low-temperature PEALD, Surf. Interfaces 27 (2021), https://doi.org/10.1016/j.surfin.2021.101559.
[53] S.M. Ognjanović, M. Winterer, Optimizing particle characteristics of nanocrystalline aluminum nitride, Powder Technol. 326 (2018) 488–497, https://doi.org/10.1016/j.powtec.2017.12.009.
[54] H. Chaurasia, S.K. Tripathi, K. Bilgaiyan, A. Pandey, K. Mukhopadhyay, K. Agarwal, N.E. Prasad, Preparation and properties of AlN (aluminum nitride) powder/thin films by single source precursor, N. J. Chem. 43 (2019) 1900–1909, https://doi.org/10.1039/C8NJ04594A.
[55] C.B. Williams, David B. and Carter, Transmission Electron Microscopy, 2012. https://doi.org/10.1016/B978-0-7020-4226-3.00022-6.
[56] S. Sharma, E.P. Amaladass, A. Mani, Defect induced magnetism and super spin glass state in reactive ion beam deposited nano-structured AlN thin films, Mater. Des. 131 (2017) 204–209, https://doi.org/10.1016/j.matdes.2017.06.020.
[57] M.A. Signore, A. Taurino, M. Catalano, M. Kim, Z. Che, F. Quaranta, P. Siciliano, Growth assessment of (002)-oriented AlN thin films on Ti bottom electrode deposited on silicon and kapton substrates, Mater. Des. 119 (2017) 151–158, https://doi.org/10.1016/j.matdes.2017.01.035.
[58] J.G. Molleja, B.J. Gómez, B. Abdallah, M. Djouadi, J. Feugeas, P. Jouan, Estudio de películas delgadas de AlN depositadas mediante sputtering por magnetrón DC en modo reactivo: efecto de la presión en la textura Study of AlN thin films deposited by DC magnetron sputtering: effect of pressure on texture, 26 (2015) 190–194.
[59] S. Mertin, B. Heinz, O. Rattunde, G. Christmann, M.A. Dubois, S. Nicolay, P. Muralt, Piezoelectric and structural properties of c-axis textured aluminium scandium nitride thin films up to high scandium content, Surf. Coat. Technol. 343 (2018) 2–6, https://doi.org/10.1016/j.surfcoat.2018.01.046.
[60] A.V. Singh, S. Chandra, A.K. Srivastava, B.R. Chakroborty, G. Sehgal, M.K. Dalai, G. Bose, Structural and optical properties of RF magnetron sputtered aluminum nitride films without external substrate heating, Appl. Surf. Sci. 257 (2011) 9568–9573, https://doi.org/10.1016/J.APSUSC.2011.06.065.
[61] C.T. Rueden, J. Schindelin, M.C. Hiner, B.E. DeZonia, A.E. Walter, E.T. Arena, K. W. Eliceiri, ImageJ2: ImageJ for the next generation of scientific image data, BMC Bioinforma. 18 (2017) 1–26, https://doi.org/10.1186/s12859-017-1934-z.
[62] X.H. Xu, H.S. Wu, C.J. Zhang, Z.H. Jin, Morphological properties of AlN piezoelectric thin films deposited by DC reactive magnetron sputtering, Thin Solid Films 388 (2001) 62–67, https://doi.org/10.1016/S0040-6090(00)01914-3.
[63] M. Ishihara, S.J. Li, H. Yumoto, K. Akashi, Y. Ide, Control of preferential orientation of AlN films prepared by the reactive sputtering method, Thin Solid Films 316 (1998) 152–157, https://doi.org/10.1016/S0040-6090(98)00406-4.
[64] B. Abdallah, S. Al-Khawaja, A. Alkhawwam, Electrical characteristics of insulating aluminum nitride MIS nanostructures, Appl. Surf. Sci. 258 (2011) 419–424, https://doi.org/10.1016/j.apsusc.2011.08.119.
[65] J.H. Choi, J.Y. Lee, J.H. Kim, Phase evolution in aluminum nitride thin films on Si (100) prepared by radio frequency magnetron sputtering, Thin Solid Films 384 (2001) 166–172, https://doi.org/10.1016/S0040-6090(00)01859-9.
[66] B. Hwang, C. Chen, H. Lu, T. Hsu, Growth mechanism of reactively sputtered aluminum nitride thin films, Mater. Sci. Eng. A 325 (2002) 380–388, https://doi.org/10.1016/S0921-5093(01)01477-0.
[67] C. Stoeckel, C. Kaufmann, R. Hahn, R. Schulze, D. Billep, T. Gessner, Pulsed DC magnetron sputtered piezoelectric thin film aluminum nitride – Technology and piezoelectric properties, J. Appl. Phys. 034102 (2014) 034102, https://doi.org/10.1063/1.4887799.
[68] H. Yang, J. Sun, H. Wang, H. Li, B. Yang, A review of oriented wurtzite-structure aluminum nitride films, J. Alloy. Compd. 989 (2024) 174330, https://doi.org/10.1016/j.jallcom.2024.174330.
[69] L. Kong, J. Zhang, H. Wang, S. Ma, F. Li, Q.M. Wang, L. Qin, Simulation study of MEMS piezoelectric vibration energy harvester based on c-axis tilted AlN thin film for performance improvement, AIP Adv. 6 (2016), https://doi.org/10.1063/1.4973648.